Journal of Nuclear Materials 379 (2008) 174–180

Contents lists available at ScienceDirect

Journal of Nuclear Materials

journal homepage: www.elsevier.com/locate/jnucmat

The long-term behaviors of passivation and hydride layer of commercial grade pure titanium in TRU waste disposal environments

Gen Nakayama [a,*], Yohei Sakakibara [a], Yoshihiro Taniyama [b], Hideo Cho [b], Takashi Jintoku [c], Susumu Kawakami [c], Mikio Takemoto [b]

[a] Research Laboratory, IHI Corporation, 1, Shin-Nakahara-Cho, Isogo-Ku, 235-8501 Yokohama, Japan
[b] College of Science and Engineering, Aoyama Gakuinn University, Japan
[c] Nuclear Power Division, IHI Corporation, Japan

ARTICLE INFO

PACS:
21.10Tg
28.41Kw
28.52Fa

ABSTRACT

Preservation of the passivity under reducing environmental conditions for extended periods of time and the behavior of hydrogen evolution as the results of the preservation of the passivity of several candidate commercial grade pure titanium related to the small amount of palladium addition, such as Ti–Gr.17 for metallic containers to be buried under deep ground for disposing of transuranic (TRU) waste is investigated. The present investigation has revealed the following corrosion paths for the titanium alloys investigated. The passivity of the alloys is preserved as the result of repeated destruction and recovery of the surface films on the alloys. The long-term corrosion rate under the preserved passivity is of the order of 10^{-6}–10^{-8} my^{-1} with evolution of hydrogen. The substrate alloys absorb parts of the hydrogen generated to form lath-type hydride phase before forming hydride layers at the final stage.

1. Introduction

Compacted hulls and end pieces are generated in the waste treatment of spent nuclear fuels, and the compacts contain transuranic (TRU) waste with the major constituent element of C-14 with the half-life period of 5730 years. The canisters for TRU waste disposal are designed to consist of corrosion-resistant layers made of commercial grade pure titanium related to the small amount of palladium addition, such as Ti–Gr.17 (Ti–0.06Pd), or titanium alloys, and the stress-bearing layers made of steel to be disposed of under the deep underground station as deep as 300 m from the ground level [1–3]. The disposal site mine galleries are constructed with concrete, and thus, the galleries are designed to be utilized at temperatures below 80 °C. Relevant analysis results indicate that although the gallery is heated to the maximum temperature of 80 °C at the initial stage of the disposal for the period less than 100 years, the temperature may converge to the ambient underground temperature of about 30 °C [1] at the disposal depth of 500 m.

The previous report [4] indicated that the target confinement period of 60,000 years for TRU waste by metal container made of Ti–0.01Pd is through to be feasible. The present investigation indicates long time behaviors of passivation and hydride layer of titanium alloy in underground water environment.

2. Long-term behavior of passivation

2.1. Evaluation of the long-term corrosion resistance

Fig. 2.1 shows the temperature dependence [5–11] of the corrosion rate of the commercial grade pure titanium when being immersed in a neutral water environment for the duration ranging from 1 to 10 months with the data of immersion tests with open circles, and those obtained by electrochemical tests with closed circles. The corrosion rates in the range of 10^{-8}–10^{-6} my^{-1}, and the rates tend to increase with increasing the test temperature. However, corrosion tests based on electrochemical procedures have the advantages to extract corrosion paths at any instant with respect to corrosion factors like the corrosion current for evaluating the corrosion rate like the current passed in titanium samples as 1 Am^{-1} = 0.86 mmy^{-1}, and the commercial grade pure titanium is found to be passivated in a wide range of the electrode potential of −0.6 to +1.0 V vs. SHE in neutral sodium water environment [12]).

2.2. The evaluation based on the destruction and recovery of the passive films

2.2.1. Time dependences of the passive current density at potentiostatic corrosion tests

Fig. 2.2(a) shows the time dependences of the passive current density of commercial grade pure titanium related to the small

* Corresponding author. Tel.: +81 45 759 2806; fax: +81 45 759 2205.
E-mail address: gen_nakayama@ihi.co.jp (G. Nakayama).

0022-3115/$ - see front matter © 2008 Elsevier B.V. All rights reserved.
doi:10.1016/j.jnucmat.2008.06.029

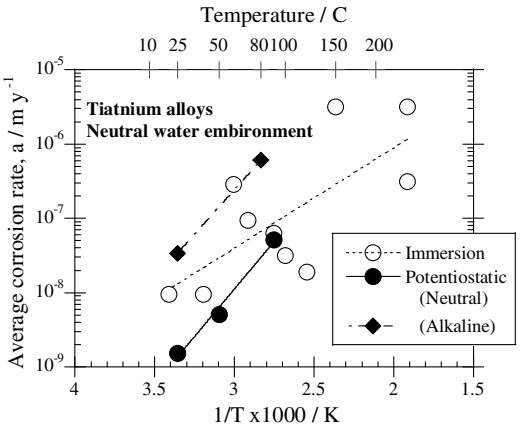

Fig. 2.1. Average corrosion rate measured by immersion tests [5–11], and by electrochemical method [12] vs. temperature of titanium alloys in neutral water environment.

amount of palladium, Ti–Gr.17 (Ti–0.06Pd) in potentiostatic tests with +0.5 V vs. SHE in concrete-permeated seawater originated water of 0.223 mol L^{-1} $[OH^-]_{all}$ +0.6 mol L^{-1} $[Cl^-]$ at 80 °C. The current density at the initial stage of the tests is of the order of 10^{-2} Am^{-2}, and it gradually decreases to the stable value of the order of 10^{-3} Am^{-2} after the test time reaches about 500 h. Furthermore, as shown in the expanded figure on the right side, the current density recovers to a steady value with some arbitrary spikes in the current density when and after loaded. These spikes of the current density are believed to be caused by the electrochemical noise signals [13] associated with the destruction and recovery of the passive surface films. The preservation of the passivity during the process of the destruction and recovery of the passive films is planned to be confirmed.

2.2.2. Dynamic destruction of passive films by loaded, scratch, indentation, tensile and pulsed laser abrasion method

2.2.2.1. Spike loaded method. The current were measured by the addition of spike loaded of 30 MPa, or 100 MPa under +0.5 V vs. SHE potentiostatic tests after the current density settled down of 10^{-3} Am^{-2} order. Fig. 2.2(b) shows the time dependences of the current. The current increases during spike loaded of 30 MPa, the current rapidly attenuates. On the other hand, the peak current is shown after unloading, even the current increase is generated under load addition. This electric charge after the unloading was consumed except for re-passivation.

2.2.2.2. Scratch method. Commercial grade pure titanium, Ti–Gr.1 test specimens are mounted with a slide stage and a corrosion cell filled with the test solution of 0.6 mol L^{-1} [NaCl] to expose the solution to the test specimens. The sliding stage is translated with a constant speed of 0.8 mm s^{-1}, and an indentation diamond piece of the Vickers hardness tester is pressed with the maximum load of 5 N while the short-circuit current between the platinum counter electrode is measured.

The changes of the shirt-circuit current at the tests are shown in Fig. 2.3. The current density corresponding to the passive state of 8×10^{-6} Am^{-1} to increase slightly with the indentation to start for 53 s in equilibrium with the ambient atmosphere, or 7 ppm dissolved oxygen, DO. The position of the scratch trace and the increase of the current are observed, and a rapid recovery occurs, or the re-passivation is induced. The total amount of the electricity at this state is about 40 μC. At the tests under the DO of 0.5 ppm, or deaerated conditions, the similar tendency is observed. However, the remaining task is to yield identical scratch at every indentation.

2.2.2.3. Indentation. Changes of the fluctuation of the electrode potential are measured when the test specimens are pressed with a diamond indenter by the load of the maximum of 100 N. The potential shifts by 13 mV in the negative direction when the load is removed, and the potential recovers gradually. The local anodic current that is computed based on the reversed potential setting method [14] for the fluctuations of the potential is 600 nA, and the electricity induced by the reaction is computed to be 290 nC.

2.2.2.4. Tensile test method. Tensile specimens are immersed in the test solution, and tensile tested with the constant crossheaded speed of 0.1 mm min^{-1}, a small fluctuation of the potential is observed when the tensile load reaches 150 MPa, and the potential gradually shifts to the less-noble direction by 23 mV. The fluctuation of the potential as observed at the fracture strain of the passive films is 0.14% based on the stress–strain curve of the alloy. The tensile load of 150 MPa that corresponds to the fracture of the passive films is quite small when compared to the yield strength of the alloy, which is 242 MPa.

2.2.2.5. Pulsed laser abrasion method. When metallic surfaces are irradiated by focused high-power laser beams, the abrasion is induced to the surfaces resulting large impacting forces. The expanding shock waves that travel on the metal surfaces induce plastic deformation on the counter metal substrate surfaces, or on the surfaces on the opposite, causing the destruction of the passive films on the opposite surfaces. The anodic current of 7 μA is detected at

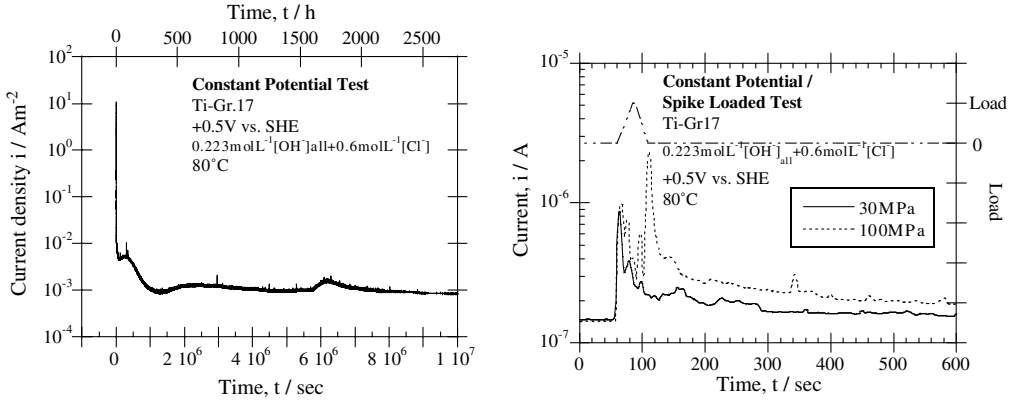

Fig. 2.2. Time dependence of passive current density of Ti–Gr.17 specimen held at +0.5 V vs. SHE in simulated concrete-permeated solution of 0.223 mol L^{-1} $[OH^-]_{all}$ +0.6 mol L^{-1} $[Cl^-]$ at 80 °C, and spike loaded effects.

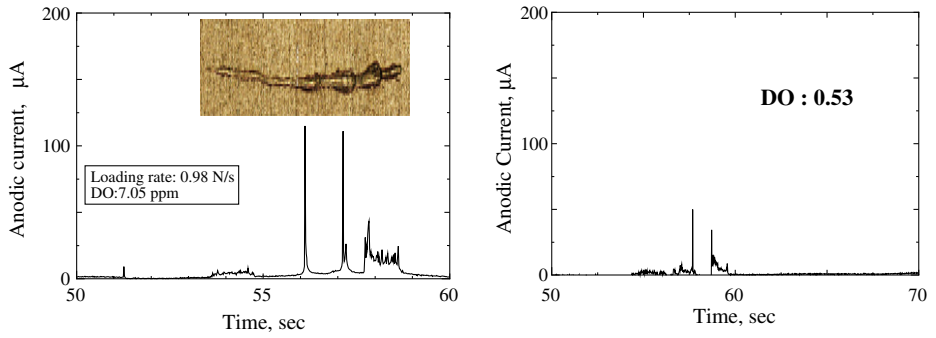

(a) Ambient environment of 7ppm DO (b) Deaerated environment of 0.5ppm DO

Fig. 2.3. Changes of anodic current of Ti–Gr.1 coupled with Pt during scratch tests with a Vickers indenter and a slide stage of 0.8 ms^{-1} speed in 0.6 mol L^{-1}[NaCl] solution.

the irradiation of the Q-switched YAG laser about 200 mJ, and the current rapidly decreases to the original value. The current returns to the original value before the laser irradiation or to the passivity preservation current density after the time of 460 s. The quantity of the electricity during this period is 51 μC, and the potential fluctuation is 70 μV.

2.2.2.6. Evaluation based on the destruction and recovery of passive films. Table 2.1 summarizes the relations between the destruction methods of passive films and the destruction and recovery processes of the passive films. Although the destruction methods of the passive films have some differences in the sensitivity, the destroyed films regain the passivity. The same tendency is confirmed to exist for the regaining the passivity under the deaerated conditions. That is to say, the titanium maintains passivity under the TRU waste disposal environment.

3. Formation of hydride layers and crack

3.1. Formation of hydride layers

Surfaces of commercial grade pure titanium preserve passive states that are induced by the presence of TiO_2 even in reducing environments. Cathodic reactions that are needed for preserving the passive states evolve a very small amount of hydrogen. A part of the atomic hydrogen in the atomic state thus produced is adsorbed and absorbed in the commercial grade pure titanium, and the remaining hydrogen recombines to form hydrogen gas, and the gas is ejected to the environmental aqueous solution. The solubility limit of hydrogen in the α-Ti alloys is as low as 20–150 ppm [15], and thus, excess hydrogen that is adsorbed and absorbed in the commercial grade pure titanium above the solubility limits forms hydride phases precipitated in the alloys. When hydrogen is absorbed at higher temperatures such as over 80 °C, hydride phases are formed uniformly in the alloys, the mechanical properties of the commercial grade pure titanium deteriorate and cause the so-called hydrogen embrittlement at the level of the hydride content above some hundreds ppm. However, the general understanding [16] is that layers of titanium hydride are formed when hydrogen is charged to the substrate alloy rapidly by the cathodic reactions at lower temperatures as under 80 °C. The absorption characteristics of hydrogen in commercial grade pure titanium, namely, the ratio of hydrogen to be absorbed to the materials, the behavior of the hydrogen, and the formation morphologies of hydrides depends on many factors including the potential, current density or hydrogen evolution rate, and temperatures.

The hydride layers thus formed and the crack formation in the layers are shown in Fig. 3.1. At the initial state, lath-type hydrides start to be formed randomly, and at a point, the layer may starts to form globular hydride phase, or hydride colony with increasing the growth of the hydride layer. The hydride layers then gradually increase the thickness, and finally, cracks are initiated in the layers.

Although the length of the initially formed individual lath-type hydride compounds is as short as a few μm. The acicular hydrides of 10–20 μm long start to grow from the alloy surfaces with increasing number of the lath-type hydride particles. The growth of the titanium hydrides is governed the diffusion of hydrogen in the hydride layers, although the diffusion rate is quite low than that in titanium. The former rate, D_H^0, in δ-$TiH_{1.6}$ is 1.33×10^{-8} m^2 s^{-1} [17] and that for the α-Ti, $D_H^0 = 5.82 \times 10^{-6}$ m^2 s^{-1} [18]. Therefore, the growth rate of the hydride particles is slower than that of newly precipitated lath-type hydride particles, and the lath-type hydride particles are enriched on the surfaces. Then, finally, the hydride layers are formed on the surfaces. The formation of the hydride layers are not restricted to the surface areas, but some hydride particles are formed as dispersed inside the alloy thickness. The acicular hydride particles that are formed at the initial stage tend to grow along deformation twins, existing [19] as shown in Fig. 3.2. Plastic deformation generates dislocations and deformation twins, and the deformation accelerates the formation of titanium hydride phases, and the formed hydride phases induce stresses in the metal matrices and thus, nuclei for hydride precipitation are generated [20]).

Table 2.1
Effects of various destruction methods of passive films on destruction and recovery processes of passive films

Test method	Destruction of passive film	0.6 mol L^{-1}[NaCl], ambient, room temp.			
		ΔE (≅V)	Δi (μA)	Q (μC)	Δt (s)
Immersion	No destruction/potentiostatic test of +0.5 V vs. SHE*	–	5.8	2.9	<600
Spike loaded	Spike loaded (30 MPa)/potentiostatic test of +0.5 V vs. SHE*	–	81.6	56.7	2340
Scratch	Slide with pressed indenter (5 N, 0.8mm s^{-1})	–	120	40	<1
Indentation	Pressed with a diamond indenter (100 N)	1000	0.6	0.3	0.4
Tensile	Constant crosshead speed tensile (0.1 mm min^{-1})	23 000	–	–	~100
Pulsed laser	Shock wave by YAG laser (200 mJ)	70	7.2	51.4	460

* 0.6 mol L^{-1} [NaCl] +0.223 mol L^{-1} $[OH^-]_{all}$, 80 °C.

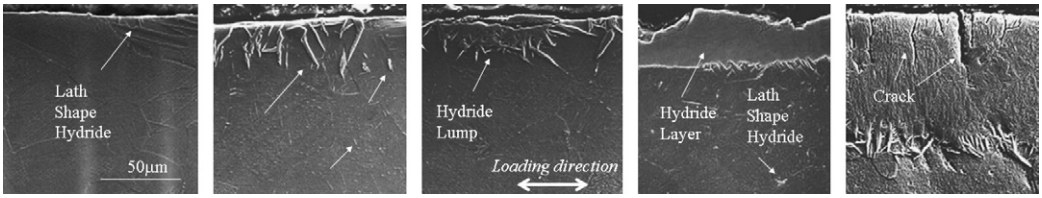

Fig. 3.1. Growth of titanium hydride phase and crack for constant load, constant current density cathodic electric charge test of 200 MPa, 0.7–30 Am^{-2}, 3–30 MCm^{-2} in 0.6 mol L^{-1}[NaCl] at 80 °C.

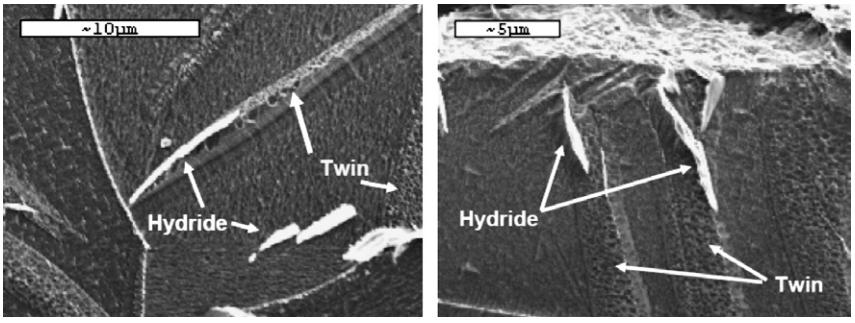

Fig. 3.2. Plate hydride produced along deformation twins in Ti–Gr.1 at hydrogen charge [19].

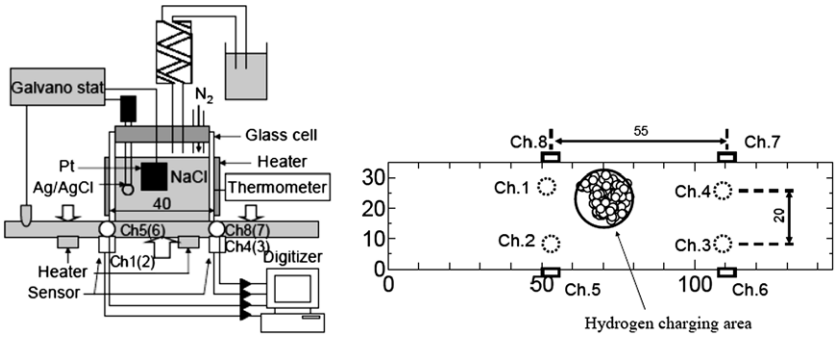

Fig. 3.3. Hydrogen charging and AE monitoring method for and from plate specimens, and AE source location estimation with AE signals detected during hydrogen charging [25].

The numbers of the hydride nuclei increases with time, and massive hydride particles are formed locally, and the density of the massive hydride precipitates increases. Thus, finally, surface hydride layers are formed, and the growth of the hydride layers toward the inside of the depth is observed [4,21–24]. Namely, the thickness of the hydride layers increases. After the thickness of the hydride layers exceeds a critical value, cracks are generated in the hydride layers. At this instant, the alloy matrices are free from diffusing hydrogen, and therefore, the microstructure is sound. Thus, the titanium matrices are not embrittled in this type of hydrogen absorption process [16].

The formation process of acicular titanium hydrides as described above can be observed by means of acoustic emission (AE). A three-point bending test specimen is corrosion tested with a corrosion cell installed on the upper surface, and a constant current electrolytic method is employed for the test. Any AE signals to be emitted from the test specimen is detected by eight AE sensors that are installed on the surface of the test specimen for monitoring the sources of the AE signals [25]). The results shown in Fig. 3.3 under the constant current with a current density of 10 Am^{-2} in an aqueous solution of 0.6 mol L^{-1} [NaCl] at 70 °C on a 2% pre-strained test specimen are explained. The AE signals observed gradually increase when the charge density exceeds 2 MC m^{-2}, and it rapidly increases at the density larger than 6 MC m^{-2}. The location of the signal sources is evaluated based on the travel time of the sound wave concerned and the sound speed in the test specimen (5990 ms^{-1}) for AE signals of larger initial frequencies. All AE signals are found to be emitted from different locations in the corrosion cell. Position of the AE signal generation is concentrated in not random position but specific position. That is to say, new acicular hydride is easy to arise in the neighborhood with pre-existing hydrides, therefore, the hydrides tend to form the colony.

3.2. Effects of environmental conditions on the formation rate of hydride phases

The cathodic current density under the aerated conditions, i_C, is due to the cathodic hydrogen evolution and that of the cathodic reduction reaction of dissolved oxygen. Thus, when the cathodic current density is sufficiently larger than the dissolved oxygen diffusion critical current density, iL_2^O, then, i_C represents the hydrogen evolution rate itself. iL_2^O is in proportion to the dissolved oxygen

concentration, CO_2, and then, corrosion tests with controlled low values of the hydrogen evolution rate, or low current density galvanostatic test can be conducted if CO_2 is kept at reduced value by applying a deaerating treatment. The experimental electrode potential for the current densities of galvanostatic tests from 0.1 to 45 Am^{-2} ranges from −1.0 to −1.3 V vs. SHE. The potential range is in the stable range for titanium hydride (TiH_2) phases on the potential – pH diagram [26], and the titanium surfaces can absorb hydrogen freely without any disturbing actions of oxide films (TiO_2) present. On the other hand, the hydrogen evolution rate for preserving passivity in ground water environments falls in the range of 10^{-3}–10^{-6} Am^{-2}. Thus, the range is the complete region for preserving passivity of TiO_2 that is near to the standard electrode potential of hydrogen gas evolution of −0.5 to −0.6 V vs. SHE.

Therefore, due to the fact that the experimental conditions are different from actual corrosion conditions, further experimental verification under extremely lower current density range, or under the conditions where the surface is completely covered by TiO_2 needs to be implemented.

Fig. 3.4 shows the relationship between the thickness of the hydride layers formed, δ_H, and the crack depth at the current density, i_C, under a constant charging of electricity [27]. As indicated in the linear by the linear relationship in the figure, the thickness of the hydride layer increases with decreasing current density. The long-term model for the hydride layer thickness [4] utilizes the relationship for the thickness of the hydride layers in terms of the current density under the current density levels for the preservation of the passive state. Under the conditions of larger current densities, for example, of the order of 40 Am^{-2}, thin hydride layers as a few μm, or thicker layers as 40 μm are formed. The majority of the data on the thick hydride layers and cracking of the layers presented in the present investigation are collected under the conditions of the large current density level.

The relationship between the formation morphology of the hydride, namely, the hydride to be formed as layers or the lath-type with the cathodic current density and the amount of electricity charged is shown in Fig. 3.5. The electricity required for the formation of hydride layers is of the order of 2 MCm^{-2}, and therefore, no hydride layer is found to be formed before a large amount of electricity is charged in the low current density region. Also involved in the figure is the relationship of the constant current tests with the charged electricity in one-year of tests, and the figure shows that one-year is required for forming hydride layers with the current density of 0.2 Am^{-2} to charge 2 MCm^{-2}. When the current density is reduced to 1/10 of the value, the time required for the formation, or the test time is extended by 10 times. Thus, plausible evaluation

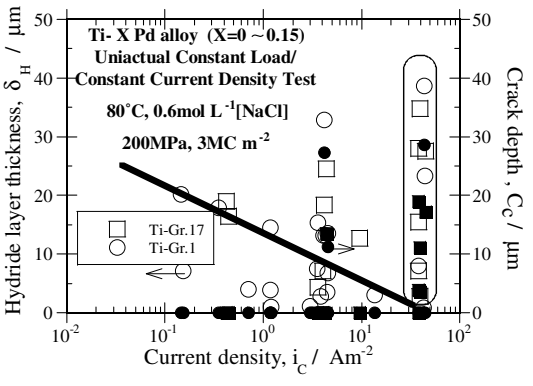

Fig. 3.4. Thickness of hydride layers and crack depth vs. current density at 80 °C in 0.6 mol L^{-1} [NaCl], 200 MPa, 3 MCm^{-2}, at constant load, and constant current density cathodic electric charge density test [27].

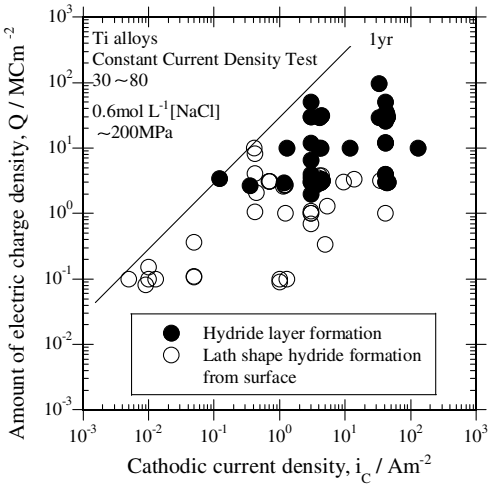

Fig. 3.5. Hydride morphology of hydride layers and lath-type hydride with respect to cathodic current density and amount of electricity density.

needs ultra-long duration of tests. However, under the existence of the surface oxide films, the hydrogen absorption is retarded, and the estimation model for the hydrogen absorption constructed based on the tests conducted in stable regions of TiH_2 is too conservative.

Based on the results presented above, tests conducted longer than dozens of years are needed for evaluating the behavior of hydride phases exposed to natural immersion conditions and simulating low accelerating corrosion environments, and tests conducted within the duration of some years would yield unsatisfactory estimation although the tests would bring self-satisfaction. Therefore, a plausible modeling is essential in presenting satisfactory estimation, and systematic studies need to be conducted.

3.3. Material characteristics of hydride layers

The crack initiation strain is investigated by conducting FEM analyses [19] with producing micro cracks in hydride phases in micro indentation tests. The two-indenter method [28] was applied with two kinds of pyramid-shaped indenters, *i.e.*, one with the apex angle of 115° and the other with 100° are indented with the load of 100 mN to the test specimens. The elastic–plastic characteristics of the hydride layers were measured based on the load and indentation distance, and the yield strength, the Young's modulus, and the work-hardening indices are determined. Furthermore, the indenters were pushed using 20 N while the fracturing of the hydride layers is detected by AE. The sign of the occurrence of micro cracking was detected at the indentation load of 19.6 N,

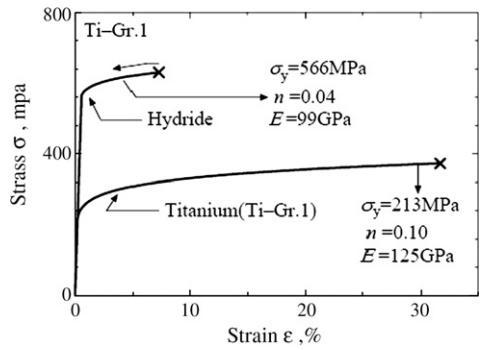

Fig. 3.6. Stress and strain curves of Ti–Gr.1 and related hydrides estimated from indentation tests [19,29].

Table 3.1
Material property of several titanium alloys and those hydride layers [19,29]

		Sample 1		Sample 2		Sample 3		Sample 4	
		B.M	Hydride	B.M	Hydride	B.M	Hydride	B.M	Hydride
Mechanical property	Hy (MPa)	292	549	213	514	270	487	239	498
	n	0.12	0.16	0.10	0.04	0.15	0.19	0.09	0.03
	E (Gpa)	105	122	125	99	94	106	107	91
	H_{max} (MPa)		849		555		718		526
	H_f (%)	38	8.1	33	4.5	54	4.3	33	16
Material	Hydride material	$TiH_{1.971}$ (07-0370)		–		TiH_2 (03-0859)		–	
		Ti–Gr.1	Commercial	Ti–Gr.1	Commercial	Ti–Gr.17	Special order	Ti–Gr.7	Labo Melt
Cathodic charge condition	Electrolysis	70 C, 0.6 mol L^{-1}[NaCl] 10 Am^{-2}, 10 MCm^{-2}		70 C, 0.6 mol L^{-1}[NaCl] 4Am^{-2}, 3MCm^{-2}		70 C, 0.6 mol L^{-1}[NaCl] 10 Am^{-2}, 10 MCm^{-2}		80 C, 0.6 mol L^{-1}[NaCl] 4 Am^{-2}, 3 MCm^{-2}	
	Stress/strain	3 PB	2% strain	UCL	100 MPa	3 PB	2% strain	UCL	200 MPa

and the indentation depth is 26.4 μm. The stress value is employed in the FEM analyses.

Fig. 3.6 shows the load-deformation curves of Ti–Gr.1 matrix and that of the hydride phase [19]. The yield stress of the hydride phases is as high as twice of that of the matrix, and the fracture strain is as low as about 8.1% of the matrix, and the fracture is brittle. The material characteristics of several titanium alloy substrates, and relevant hydride phases are listed in Table 3.1 [19,29]. The yield strength of the hydride is about twice of that of the substrate alloys, and the fracture strain is extremely small. As shown in Section 2.2.2, the fracture stress of TiO_2 oxide films is of the order of 150 MPa. The alloys tested are commercially available plates of Ti–Gr.1, Gr.17 and Gr.7 with those of especially order-melted plates, and of laboratory melted and rolled plates. The alloys have different Pd contents, different controls of impurities like O and F, and different rolling and heat-treatment sequences. The formation conditions of the hydride phases are not identical as well.

Under the conditions that the yield strength of those commercial grade pure titanium not related to the small amount of palladium addition is of the order of 200 MPa (0.2% endurance strength is 167–294 MPa), and the stress imposed on metal vessels from residual stresses is assumed to be of the same order, the tensile stress applied on hydride layers is only one half of the endurance strength. Therefore, most of the fracturing of the hydride layers is induced by the internal stress to be generated by the formation of the hydride phases accompanying some degrees of volume expansion.

SIMS analyses [30] were conducted on specimens containing hydride phases by constant load and constant current tests in neutral salt aqueous solutions for analyzing the hydrogen concentration profiles in the cross-sections of the galvanostatically charged titanium alloy test specimens with hydrogen. The data obtained [31] show that the surface oxide films contain a large amount of hydrogen, and that a definite concentrations profile of hydrogen is observed to exist in the specimen thickness direction in the hydride layers. The results indicate that the hydride phases have different hydrogen concentration with respect to the thickness as $1.54 < n < 2.0$, and $n = 2$ on the surface for TiH_n, and the value of n becomes smaller with increasing depth in the thickness direction [30]. The decrease of the value of n of the hydride phases indicates the decrease of the hydrogen content in the hydride layers, accompanying with changes of dynamic characteristics of the hydride layers. The higher hydrogen content induces brittle nature, and complicated crack morphologies including the spalling or flaking of surface hydride layers may be induced.

3.4. Formation of hydride layers and cracking behavior of the layers

The hydrogen absorbed at relatively lower temperatures below 80 °C forms a lath-type hydride phase. The lath-type hydride particles are formed preferentially at high strain fields like twins, and the strain fields are induced by pre-existing hydride particles that precipitated beforehand, and thus, hydride phases tend to be formed at sites adjacent to pre-existing hydride particles. The diffusion rate of hydrogen is higher in metallic titanium than in hydrides, and thus, the formation of hydride phases is preferred than the growth of the existing hydride phases. Thus, globular hydride phases are often formed, and the globular hydrides tend to change the morphology to the layered form. Even in a layer of the hydride, there exists a concentration gradient of hydrogen, and in the layer in the thickness direction. The outer part of the layer tends to be TiH_2, that is the highest in hydrogen, and is brittle than the inner part of the layer. This is the most exciting nature of the formation of the hydride layers, and therefore, the estimation of the embrittlement of the layers based on the mean hydrogen concentration of the layer would be problematic.

4. Conclusions

The long-duration preservation of the passive state of commercial grade pure titanium in aqueous environments of concrete-permeated deep level groundwater, and the behavior of hydrogen evolution during the preservation are investigated in details. The following conclusions are obtained.

(1) Ti–Gr.1 and Ti–Gr.17 (Ti–0.06Pd) are passivated in the neutral water environments. The corrosion rates of the metals induced by the preserving the passivity is on the order of 10^{-8}–10^{-6} my^{-1}, and the amounts of corrosion can be computed based on the time integrals of the values. With increasing environmental temperature and $[OH]_{all}$, the corrosion rate tends to increase. The metal and the alloys are found to be passivated even in reducing environments.
(2) The titanium maintains passivity under the TRU waste disposal environment, even dynamic destruction of passive films were done by loaded, scratch, indentation, tensile and pulsed laser abrasion method.
(3) The hydrogen absorbed at relatively lower temperatures below 80 °C forms a lath-type hydride phase. The lath-type hydride particles are formed preferentially at high strain fields like twins, and the strain fields are induced by pre-existing hydride particles that precipitated beforehand, and thus, hydride phases tend to be formed at sites adjacent to pre-existing hydride particles. Thus, globular hydride phases are often formed, and the globular hydrides tend to change the morphology to the layered form.
(4) The strain need for generating cracks was investigated by forming cracks with micro indentation tests for understanding the material characteristics of the hydride layers with the help of the FEM analyses. The yield strength of the

hydride phases is as high as twice of that of the substrate alloys, and the fracture strain is as low as about 8.1% with a brittle manner. The brittle nature of the hydride layers induces the brittle crack formation in the hydride layers.

References

[1] Progress Report on Disposal Concept for TRU Waste in Japan, Japan Nuclear Cycle Development Institute and The Federation of Electric Power Companies, JNC TY1400 2000-002/TRU TR-2000-02, 2000.
[2] H. Sakamoto, S. Kobayashi, H. Tanabe, S. Kataoka, T. Yoshida, A. Takei, Y. Nakamori, M. Sugimoto, T. Kanno, in: Proceedings of International Conference on Back-End of the Fuel Cycle, Global 2001, Paris, France, 2001.
[3] Progress Report on Disposal Concept for TRU Waste in Japan – 2nd Report, Japan Nuclear Cycle Development Institute and The Federation of Electric Power Companies, JNC TY1400 2005-013/TRU TR-2005-02, 2005.
[4] G. Nakayama, Y. Fukaya, M. Akashi, S. Sawa, T. Kanno, H. Owada, A. Otsuki, H. Asano, in: Proceedings of the Second International Workshop, Prediction of Long Term Corrosion Behaviour in Nuclear Waste Systems, NICE, September 2004, EUROCORR2004, p. 35–44, European Federation of Corrosion, 2004.
[5] H. Mattson, I. Olefjord: SKB Tech. Report 84-19, 1984.
[6] S.G. Pitman, ASTM STP 830, ASTM, 1984, p. 5.
[7] M.A. Molecke, J.A. Ruppen, R.B. Diegle, Nucl. Technol. 63 (1983) 476.
[8] S. Henriksson, K. Pettersson, SKB Report, No. 11, Sweden, 1977.
[9] S. Matsuno, Review of Tokyo Dental College Society (Jpn.) 87 (1987) 1141–1152.
[10] W.H. Smyrl, L.L. Stephenson, J.W. Braithwaite: CORROSION/97, Paper No. 85, NACE, 1977.
[11] S. Henrikson, M. Pourbaix, SKB Tech. Report, SKB-Tr-96, Stockholm, 1978.
[12] Y. Fukaya, M. Akashi, CORROSION/2003, Paper No. 680, NACE International, 2003.
[13] K. Yamakawa, H. Inoue, Life Prediction of Corrodible Structures, vol. II, NACE, 1994. p. 992.
[14] H. Inoue, Zairyo-to-Kankyo (Jpn.) 52, JSCE, 2003, p. 444.
[15] N.E. Paton, J.C. Williams, in: I.M. Bernstein, A.W. Thompson (Eds.), Hydrogen in Metals, ASM, 1974, pp. 409–431.
[16] K. Shimogoori, #47th Corrosion and Protection Symposium (Jpn.), JSCE, 1982, p. 23.
[17] J.O'M. Bockris, A.K.N. Reddy, Modern Chemistry, McDonald, London, 1970.
[18] NBS data, J. Phys. Chem. Ref. Data 11(Suppl. 2), 1982.
[19] H. Koketsu, Y. Taniyama, A. Yonezu, H. Cho, T. Ogawa, N. Takemoto, G. Nakayama, Zairyo-to-Kankyo (Jpn.), vol. 55, Japan Society of Corrosion Engineering, 2006.
[20] C.J. Carpenter, J.F. Eatters, J. Nucl. Mater. 73 (1978) 190.
[21] I.I. Phillips, P. Poole, L.L. Shreir, Corros. Sci. 14 (1974) 533.
[22] T. Mizuno, K. Shindo, T. Morozumi, Bosyoku-Gizyyutu (Jpn.) 26 (1977) 185.
[23] R. Gruner, B. Streb, E. Brauer, Hydrogen in Titanium, in: Proceedings of Fifth International Conference on Titanium, Deutsche Gesekkschaft fur Metallkunde E.V., 1985, p. 2571.
[24] Z.F. Wang, C.L. Briant, K.S. Kumar, Corrosion 54 (1998) 553.
[25] Y. Takeyama, T. Matsuo, H. Cho, M. Takemoto, G. Nakayama, Progress in Acoustic Emission XIII, Paper No. 295, The Japanese Society for NDI, 2006.
[26] M. Pourbaix, Werks. Korr. 11 (1960) 761.
[27] G. Nakayama, K. Murakami, M. Akashi, MRS Proc. Vol. 757, II4-11, MRS, 2002.
[28] M. Dao, N. Chollacoop, K.J. Van Vliet, T.A. Venkatesh, S. Suresh, Acta Mater. 49 (2001) 3899.
[29] Y. Taniyama, H. Cho, T. Ogawa, G. Nakayama, M. Takemoto, J. Mater. Sci. Soc. Jpn. 44 (2006) 106.
[30] T. Mizuno, M. Nobuoka, in: Proceedings of the 42 Japan Conference Materials and Environments (Jpn.), JESC, 1995, p. 561.
[31] N. Nakamura, M. Akashi, Y. Fukaya, G. Nakayama, CORROSION 2000, Paper No. 195, NACE International, 2000.